

s-wave superconductivity in the noncentrosymmetric W_3Al_2C superconductor: An NMR study

D Tay¹, T Shang^{2*}, Y P Qi³, T P Ying^{4,5}, H Hosono⁴, H-R Ott^{1,6}, and T Shiroka^{1,6*}

¹Laboratorium für Festkörperphysik, ETH Zürich, CH-8093 Zurich, Switzerland

²Key Laboratory of Polar Materials and Devices (MOE), School of Physics and Electronic Science, East China Normal University, Shanghai 200241, China

³School of Physical Science and Technology, ShanghaiTech University, Shanghai 201210, China

⁴Materials Research Center for Element Strategy, Tokyo Institute of Technology, Yokohama 226-8503, Japan

⁵Beijing National Laboratory for Condensed Matter Physics, Institute of Physics, Chinese Academy of Sciences, Beijing 100190, China

⁶Paul Scherrer Institut, CH-5232 Villigen PSI, Switzerland

E-mail: tshiroka@phys.ethz.ch, tshang@phy.ecnu.edu.cn

Abstract. We report on a microscopic study of the noncentrosymmetric superconductor W_3Al_2C (with $T_c = 7.6$ K), mostly by means of ^{27}Al - and ^{13}C nuclear magnetic resonance (NMR). Since in this material the density of states at the Fermi level is dominated by the tungsten's $5d$ orbitals, we expect a sizeable spin-orbit coupling (SOC) effect. The normal-state electronic properties of W_3Al_2C resemble those of a standard metal, but with a Korringa product $1/(T_1T)$ significantly smaller than that of metallic Al, reflecting the marginal role played by s -electrons. In the superconducting state, we observe a reduction of the Knight shift and an exponential decrease of the NMR relaxation rate $1/T_1$, typical of s -wave superconductivity. This is further supported by the observation of a small but distinct coherence peak just below T_c in the ^{13}C NMR relaxation-rate, in agreement with the fully-gapped superconducting state inferred from the electronic specific-heat data well below T_c . The above features are compared to those of members of the same family, in particular, Mo_3Al_2C , often claimed to exhibit unconventional superconductivity. We discuss why, despite the enhanced SOC, W_3Al_2C does not show spin-triplet features in its superconducting state and consider the broader consequences of our results for noncentrosymmetric superconductors in general.

Keywords: Noncentrosymmetric superconductors, electronic correlations, s -wave superconductivity, NMR

Submitted to: *J. Phys.: Condens. Matter*

1. Introduction

Noncentrosymmetric superconductors (NCSCs) belong to a class of materials that miss a key symmetry, such as parity [1]. In NCSCs, the lack of inversion symmetry of the crystal lattice often induces an antisymmetric spin-orbit coupling (ASOC), which lifts the degeneracy of the conduction-electron bands and splits the Fermi surface. Consequently, both intra- and inter-band Cooper pairs can be formed and an admixture of spin-singlet and spin-triplet pairings is possible. The extent of the singlet-triplet admixture is notably determined not just by the strength of the ASOC, but also by other microscopic parameters [1, 2]. In superconductors with spin-triplet pairing, time-reversal symmetry (TRS) breaking is not a strict requirement [3]. Hence, they are particularly interesting for studying TRS, should it occur [1]. A notable example is that of UPT_3 , where claims of triplet superconductivity (SC) have been confirmed by various experimental methods [4], including measurements of zero-field muon-spin relaxation [5] and optical Kerr effect [6].

A particular NCSC family, which exhibits unconventional superconducting properties, is that of M_3X_2Y compounds. For the definition of “unconventional” superconductor (basically one that does not conform to *s*-wave pairing), we follow the definition put forward in ref. [7]. Here, $M = Mo, Pd, W, Pt$; $X = Li, Al$; and $Y = B, C, N$. Five members of this family have already been studied and, in ascending order of atomic number Z of the metal atom M , they are: Rh_2Mo_3N , Mo_3Al_2C , Li_2Pt_3B , W_3Al_2C , and Li_2Pd_3B . From general principles, it is expected that as Z increases, the ASOC strength increases as well. Consequently, a superconductor of an unconventional type is more likely to appear in metals with a higher atomic number. Indeed, from the existing literature, it is known that, while Li_2Pd_3B is a conventional superconductor [8], its high- Z Pt counterpart, Li_2Pt_3B , exhibits unconventional superconductivity [9], here identified by the presence of gap nodes [10]. The superconducting properties of the isostructural Mo_3Al_2C vs W_3Al_2C compounds are, however, still under study, with various groups reporting clearly contradictory types of superconductivity, for either of them, both conventional [11, 12, 13, 14, 15, 16, 17] and unconventional [18, 19]. Thus, in Mo_3Al_2C , a power-law behavior of the ^{27}Al NMR spin-lattice relaxation rates possibly suggests superconducting gap nodes [18], while the exponential temperature dependence of the magnetic penetration depth and the absence of time-reversal symmetry breaking are more consistent with conventional nodeless

SC [16, 20]. More experimental data is required to fully establish the behavior of these systems.

In this paper, we explore the electronic properties of W_3Al_2C , in both the normal- and the superconducting states. Our results indicate that this system is only weakly correlated. Most importantly, based on our NMR experiments, we provide evidence of BCS-type *s*-wave pairing in the noncentrosymmetric W_3Al_2C superconductor. It is surprising that unconventional superconductivity is not observed, even though W has a higher atomic number than Mo (and, hence, a larger ASOC). We argue why, despite the presence of the heavier element, W_3Al_2C exhibits only conventional SC behaviour.

2. Experimental details

Polycrystalline samples of W_3Al_2C were prepared via high-temperature, high-pressure solid-state reaction. To achieve a homogeneous mixture, high-purity W, Al, and C powders in a quasi-stoichiometric ratio 3:1.8:0.8 were ball-milled for two days in a glove box under Ar atmosphere. The mixture was then pressed into a pellet and placed in an *h*-BN capsule, where the sample was heated up to 2173 K under 5 GPa for 24 hours. Room-temperature x-ray powder diffraction (XRD) measurements were performed in a Bruker D8 diffractometer with Cu $K\alpha$ radiation. Rietveld refinements via the FULLPROF suite confirm the cubic structure of W_3Al_2C , with a space group $P4_132$ (No. 213) [22]. Magnetic susceptibility and heat-capacity measurements were performed on, respectively, a vibrating sample magnetometer (VSM) and a physical property measurement system (PPMS), both by Quantum Design. Further details on sample preparation and characterization have been reported in [11].

The ^{27}Al NMR measurements, including lineshapes and spin-lattice relaxation times, were performed on W_3Al_2C in powder form in different applied magnetic fields (4–7 T). To cover the 1.8 to 300 K temperature range we used a continuous-flow CF-1200 cryostat by Oxford Instruments, with temperatures below 4.2 K being achieved under pumped 4He conditions. Preliminary resonance detuning experiments confirmed a T_c of 7.6 K at 0 T (5.3 K at 5 T). The ^{27}Al NMR signal was detected by means of a standard spin-echo sequence, consisting of $\pi/2$ and π pulses of 3 and 6 μs , with recycling delays ranging from 1 to 60 s, in the 1.8–300 K temperature range. Despite an echo delay of 100 μs , 2 to 32 scans were sufficient to acquire a good-quality signal. The lineshapes were obtained via fast Fourier transform (FFT) of the echo

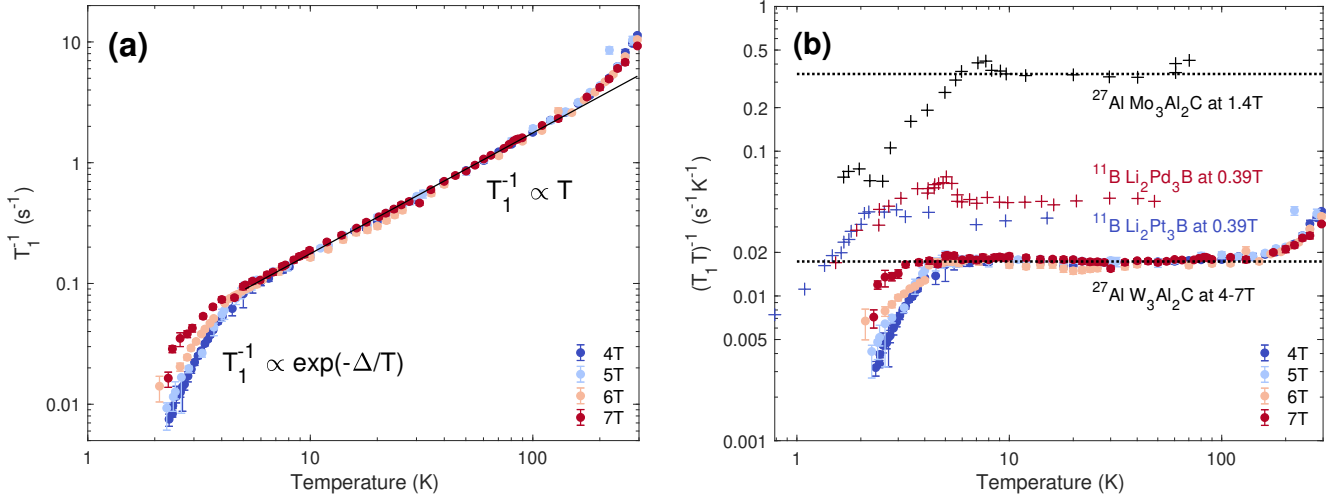


Figure 1. (a) $1/T_1$ vs temperature measured in different fields. Above T_c , the field independent spin-lattice relaxation rate is linear in temperature and changes slope at $T^* \sim 103$ K. (b) $1/T_1 T$ vs temperature. For $T > T_c$ (here 5.3 K), the product is almost constant ($0.017 \text{ s}^{-1} \text{ K}^{-1}$). For comparison, we also show the data for Mo_3Al_2C [14], Li_2Pd_3B [21] and Li_2Pt_3B [21] — see text for the discussion.

signal. Spin-lattice relaxation times T_1 were measured via the inversion recovery method, using a $\pi-\pi/2-\pi$ pulse sequence. Subsequently, the T_1 values for the central transition of the spin- $5/2$ ^{27}Al nucleus were obtained by using the relevant formula for the relaxation of quadrupole nuclei [23].

3. Results and discussion

3.1. ^{27}Al NMR in the normal- and superconducting phases

NMR is a powerful local technique for investigating the electronic properties of materials, in particular, their electronic correlations, magnetic order, and superconductivity [24]. Although the magnetic field reduces the T_c value, a high upper critical field (above 50 T [12]), still allows us to explore the superconducting behaviour of W_3Al_2C . In addition, we also investigated the NMR response in the normal state. The ^{27}Al NMR measurements were performed in different external magnetic fields, from 4 to 7 T, corresponding to T_c values between 5.9 K and 4.6 K. In all cases, the ^{27}Al NMR reference frequency ν_0 was calculated with respect to a standard $Al(NO_3)_3$ reference. The T_1 relaxation times were calculated by using a stretched-exponential relaxation model [23, 25], whereby disorder is modelled by a stretching coefficient β :

$$\frac{M_z(t)}{M_z^0} = 1 - f \left(\frac{1}{35} e^{(-t/T_1)^\beta} + \frac{8}{45} e^{(-6t/T_1)^\beta} + \frac{50}{63} e^{(-6t/T_1)^\beta} \right)$$

Here M_z^0 is the magnetization value at thermal equilibrium, while f reflects the efficiency of population inversion (ideally 2). In general, the experimental NMR data — shifts and relaxation rates — clearly reflect the two phases of W_3Al_2C : a normal metallic phase above T_c and a BCS-type superconducting phase below it.

3.1.1. Metallic behaviour in the normal phase

In the normal phase, we observe an almost ideal metallic behaviour for all the applied magnetic fields (see figures 1(a) and 2(b)). For instance, the relaxation-rate data in figure 1(a) are well described by a power-law function with a scaling exponent of 1.0(1), i.e., the relaxation rate is perfectly proportional to temperature. We can also compute the Korringa product $1/T_1 T$ (here, only $0.017 \text{ s}^{-1} \text{ K}^{-1}$), which is proportional to the electronic density of states at the Fermi level, $N(E_F)$ (see figure 1(b)). As expected for an ideal metal, in the normal phase of W_3Al_2C , $N(E_F)$ is practically constant with temperature and independent of the applied magnetic field, but approximately thirty times smaller than the Korringa product in metallic Al ($0.54 \text{ s}^{-1} \text{ K}^{-1}$) [26, 27]). These widely differing relaxation rates are partly reflected also in the different Knight shifts: 450 ppm in W_3Al_2C vs 1636 ppm in metallic Al [28], resulting in a $T_1 T K^2$ of $1.19 \times 10^{-5} \text{ sK}$ and $4.98 \times 10^{-6} \text{ sK}$ in W_3Al_2C and in metallic Al, respectively. The different $T_1 T K^2$ values suggest that, although W_3Al_2C is an ordinary metal in its normal phase, it could still exhibit weak electronic correlations. The strong reduction in shift in W_3Al_2C suggests a very small contribution of *s*-electrons (responsible for the contact hyperfine interaction) at the Fermi energy. This is consistent with previous NMR studies of Al-based alloys [29] and with the electronic structure calculations of W_3Al_2C [11]. Indeed, the latter indicate that the *s*-electron band is shifted to higher energies, whereas the valence *d*-electron band of the W transition metal is prominent at the Fermi level.

3.1.2. NMR evidence of BCS superconductivity in W_3Al_2C

In the superconducting phase, the electronic properties of the system can be described by the standard BCS

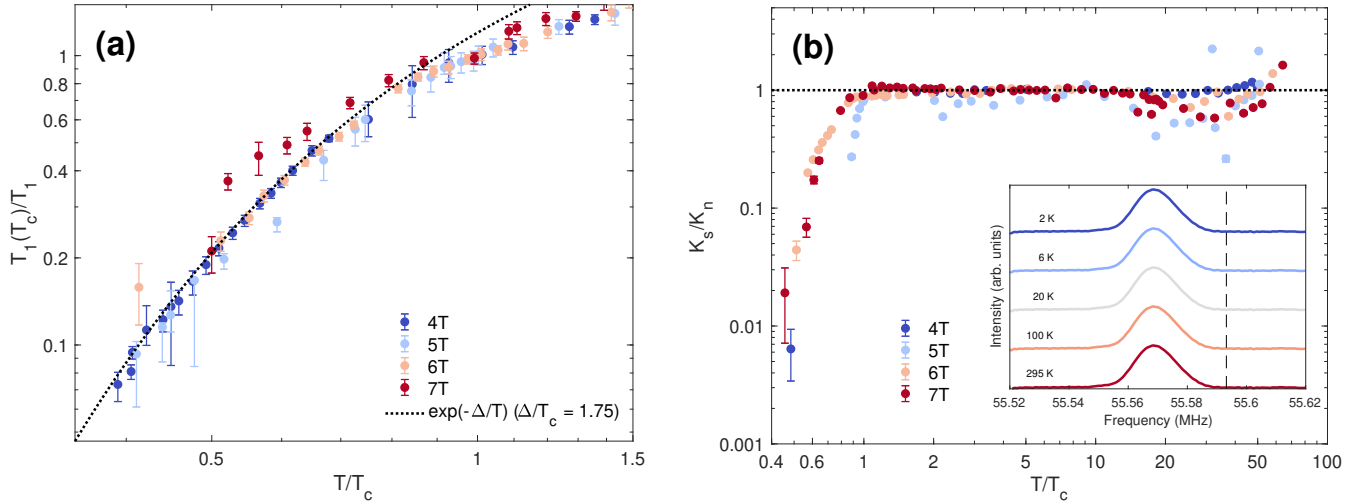


Figure 2. Evidence of conventional BCS superconductivity in W_3Al_2C . (a) Below T_c , the relaxation rate (T_1^{-1}) can be described by a single-gap exponential function $\exp(-\Delta/T)$. (b) The NMR shift K_s (scaled by its normal-state value K_n at T_c) remains constant down to T_c , but decreases sharply below it. Inset: ^{27}Al NMR line shapes at selected temperatures measured in a 5-T applied magnetic field. The vertical line indicates the reference frequency ν_0 . Above T_c , the lineshapes are practically temperature-independent.

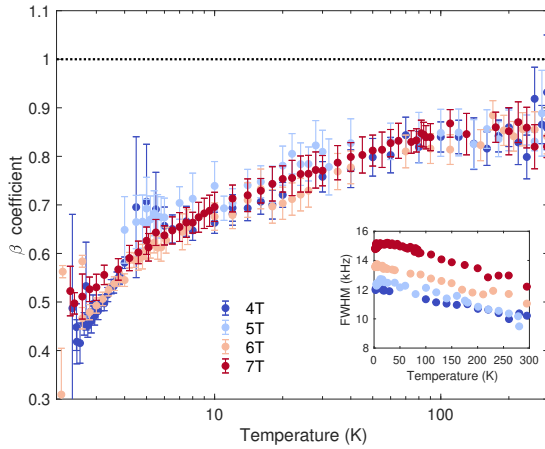


Figure 3. Temperature dependence of the stretching coefficient β . Inset: Temperature dependence of the linewidth. The behaviour of both parameters suggests the presence of intrinsic disorder in W_3Al_2C .

theory, which predicts a gap ratio $2\Delta_0/k_B T_c = 3.53$ (see figure 2(a)) and a reduction of the NMR shift at low temperatures (see figure 2(b)). Here, the reduced shift reflects an electron pairing forming spin-compensated (typically *s*-wave) Cooper pairs. This result is consistent with a recent muon-spin rotation (μ SR) study of W_3Al_2C [12], where *s*-wave superconductivity with the same gap ratio was reported. The superconducting gap value we find in W_3Al_2C is similar to the *average* SC gap reported in Mo_3Al_2C , where an NMR study claimed a $2\Delta_0/k_B T_c$ ratio of 2.8(2) [14], while specific-heat measurements implied a ratio of 4.03 [13].

3.1.3. Detection of the Hebel-Slichter peak via ^{13}C NMR

According to the Korringa relation [30], T_1 in metals depends strongly on $N(E_F)$. Hence, upon entering the superconducting state, we expect an exponential decay of T_1 . Yet, preceding this decay, just below T_c the spin-lattice relaxation rate first increases above its normal-state Korringa value, showing a so-called coherence (or Hebel-Slichter — HS) peak [31, 32]. Such increase in relaxation rate results partly from the enhanced density of electronic states, which pile up near the SC gap edges [33, 34]. Considering its key role in the experimental confirmation of the BCS theory, the observation of a Hebel-Slichter peak is recognized as a clear indication of BCS-type *s*-wave superconductivity.

However, its absence does not necessarily rule out the possibility of a standard *s*-wave pairing. This seems to be also the case for W_3Al_2C where, as illustrated in figure 1(a), we do not observe the expected peak in the ^{27}Al NMR relaxation rates below T_c . Several hypotheses can be put forward to explain this experimental result.

One possibility, relevant to type-II superconductors, was suggested by Goldberg and Weger [35]. Here, the total nuclear spin-relaxation rate consists of the sum of two terms, the first of which describes the relaxation in the normal-state vortex cores, while the other captures the relaxation in the remaining superconducting volume. This theory predicts that the contribution from the normal-state cores is proportional to the external magnetic field H . To test it, we measured the relaxation rates at different magnetic fields, in the range from 4 to 7 T. As can be seen in figure 2(a), the (scaled) relaxation times generally fall on the same exponential curve, indicating that no field-dependent term arises from vortex cores. Consequently, this hypothesis cannot explain the absence of an HS peak.

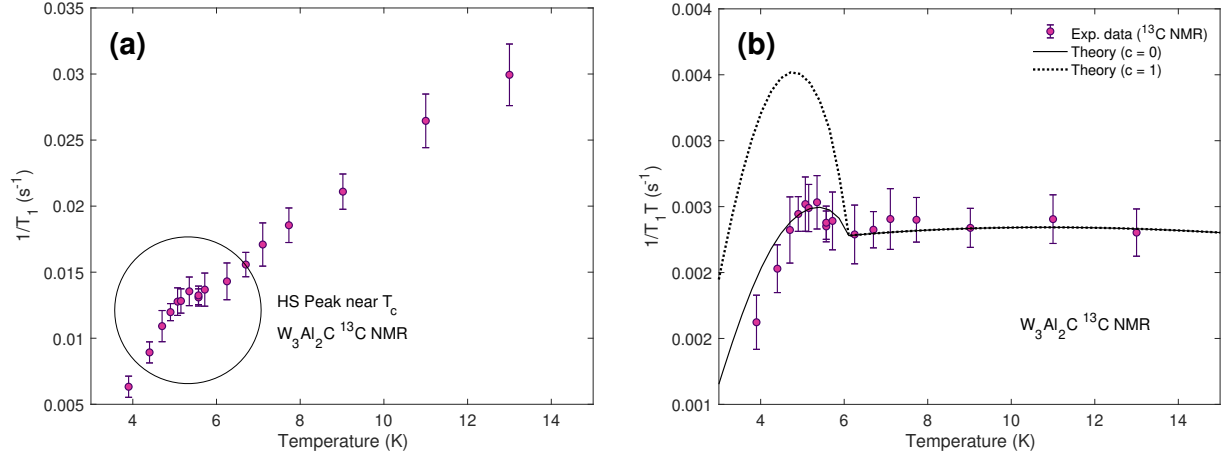


Figure 4. ^{13}C NMR relaxation data in W_3Al_2C . Temperature dependence of the relaxation rate T_1^{-1} (a) (the HS peak is circled in black) and of the Korringa product $(T_1 T)^{-1}$ (b). Fits to equation (1) are also shown for the $c = 0$ and $c = 1$ cases (see text for details).

Another possibility is that the HS peak is suppressed by disorder, caused by intrinsic defects and/or magnetic impurities. To investigate the role of disorder, we studied the linewidths and the stretching coefficient β . As shown in figure 3, β decreases continuously as the temperature is lowered, while remaining always smaller than 1. This indicates a distribution of relaxation rates, reflecting the inequivalence of NMR sites, in turn due to the intrinsic disorder (see, for instance, refs. [36, 37]). However, we find that both parameters depend only weakly on temperature and show no discontinuities or an unusual behaviour near T_c . Thus, we can rule out the possibility that disorder, although present, is affecting the HS peak.

Yet another possibility is that, for quadrupolar nuclei such as the spin-5/2 ^{27}Al , also the quadrupole interaction contributes to the spin-lattice relaxation, tending to smear out the HS peak [38]. To test this possibility, we measured the ^{13}C NMR relaxation rate in W_3Al_2C . Since ^{13}C is a spin-1/2 nucleus, it represents a purely dipolar probe, not undergoing any quadrupole interaction. As can be seen in figure 4(a), we indeed observe a small feature just below T_c . Here, the exact T_c value at 5 T was determined by means of a standard resonance-detuning experiment (data not shown).

To model the feature near T_c , we begin with the usual expression for the HS peak [33]:

$$\frac{R_s}{R_n} = \frac{2}{k_B} \int_{\Delta}^{\infty} [N_s^2(E) + M_s^2(E)] f(E) [1 - f(E)] dE. \quad (1)$$

Here, R_s and R_n are the relaxation rates in the superconducting and the normal state, respectively, $M_s(E) = N_0 \Delta / \sqrt{E^2 - \Delta^2}$ is the anomalous density of states (DOS) due to the coherence factor [33], and $N_s(E) = N_0 E / \sqrt{E^2 - \Delta^2}$ is the DOS in the superconducting state.

In our case, two modifications were made. Firstly, we chose to convolute $M_s(E)$ and $N_s(E)$ with a triangular broadening function $B(E)$, characterized by a width 2δ

and a height $1/\delta$, with $\delta = 0.2\Delta$. Secondly, we model the degree of coherence by the parameter c , by making the substitution $\Delta \rightarrow c\Delta$. The conventional BCS theory [39] predicts that, depending on the details of the scattering operator, the scattering matrix element can adopt a positive or a negative sign. The modelling of the HS peak typically requires a positive sign, but in other situations, e.g., in ultrasound absorption, the negative sign has to be used. Here, by setting c as an adjustable parameter, one can model the case where the scattering matrix consists of both positive and negative components, which may cause a (partly) suppression of the HS peak. After these two modifications, $N_s(E)$ and $M_s(E)$ can be written as [40]:

$$N_s(E) = \int B(E' - E) \frac{E'}{(E'^2 - \Delta^2)^{1/2}} dE', \quad (2)$$

$$M_s(E) = \int B(E' - E) \frac{c\Delta}{(E'^2 - \Delta^2)^{1/2}} dE'. \quad (3)$$

The fit results are shown in figure 4(b). We find that the fit obtained by fixing $c = 1$ drastically overestimates the relaxation rates below T_c . On the other hand, the fit obtained by fixing $c = 0$ reproduces adequately the feature near T_c , although with a slightly overestimated relaxation below T_c .

From the ^{13}C NMR relaxation rates in the superconducting state and the above analysis we infer with some confidence that W_3Al_2C indeed exhibits *s*-wave superconductivity, as evidenced by the observation of an (albeit reduced) HS peak. Yet, it appears that there are some decoherence effects, both at and below T_c , most likely due to a strong electron-phonon coupling in this material (see ref. [41] and the section below). In general, the exact mechanism of such decoherence effects is yet to be understood.

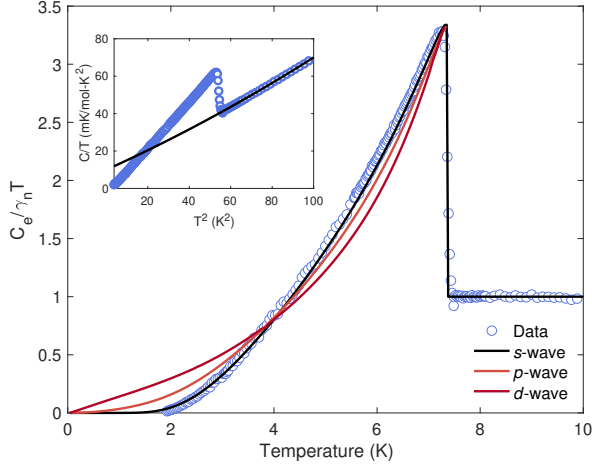


Figure 5. Normalized electronic specific heat $C_e/\gamma T$ for W_3Al_2C versus temperature. Inset: The measured specific heat C/T as a function of T^2 . The dashed line in the inset is a fit to $C/T = \gamma + \beta T^2 + \delta T^4$, yielding $\gamma = 10(1)$ mJ/mol-K², $\beta = 0.49(4)$ mJ/mol-K⁴, and $\delta = 1.0(3) \times 10^{-3}$ mJ/mol-K⁶. The solid lines in the main panel are the electronic specific heat calculated by considering *s*-, *p*- and *d*-wave models. Specific heat data were taken from ref. [11].

3.2. Electronic specific heat

To get further insight into the superconducting state of W_3Al_2C , the temperature dependence of its electronic specific heat was evaluated and analyzed using different models. After subtracting the phonon contribution from the measured specific heat (see inset in figure 5), the electronic specific heat divided by the electronic specific-heat term, i.e., $C_e/\gamma T$, is obtained and presented in figure 5. The temperature-dependent superconducting-phase contribution to the entropy was calculated by means of the expression [42]:

$$S(T) = -\frac{6\gamma_n}{\pi^2 k_B} \int_0^\infty [f \ln f + (1-f) \ln(1-f)] d\epsilon, \quad (4)$$

where γ_n is the normal-state electronic specific-heat coefficient, $f = (1 + e^{E/k_B T})^{-1}$ is the Fermi function and $E(\epsilon) = \sqrt{\epsilon^2 + \Delta^2(T)}$ is the excitation energy of quasiparticles, with ϵ the electron energies measured relative to the chemical potential (Fermi energy) [42, 47]. Here, $\Delta(T)$ is the temperature dependent gap function, which in the BCS *s*-wave model can be written as $\Delta(T) = \Delta_0 \tanh\{1.82[1.018(T_c/T - 1)]^{0.51}\}$ [48], with Δ_0 the gap value at zero temperature. In case of *p*- and *d*-wave models, the temperature-dependent gap functions are $\Delta(T)\sin\theta$, and $\Delta(T)\cos 2\phi$, respectively, exhibiting point- and line nodes in the respective gap function. The temperature-dependent electronic specific heat in the superconducting state can be calculated from $C_e = T \frac{dS}{dT}$.

The fit results using the above-mentioned models are shown by solid lines in the main panel of figure 5. We find that, while the *s*-wave model fits the electronic specific heat data across the entire temperature range,

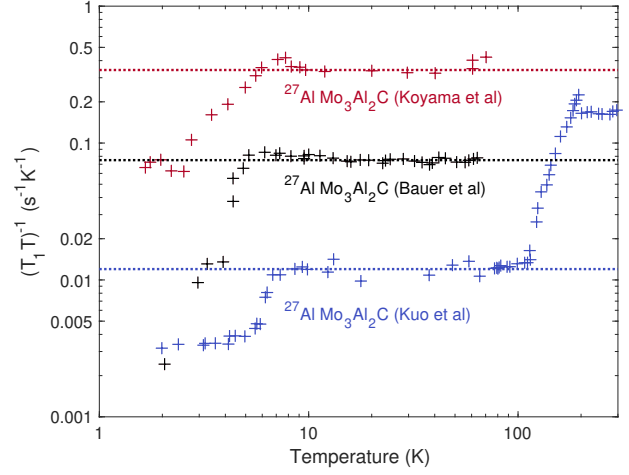


Figure 6. $1/T_1 T$ vs temperature for Mo_3Al_2C as obtained from Koyama et al [14], Bauer et al [18] and Kuo et al [19]

the *p*- and *d*-wave models deviate significantly from the data, implying the absence of any gap nodes in the superconducting state of W_3Al_2C . The fully-gapped *s*-wave model gives a superconducting gap $\Delta_0 = 2.25(5) k_B T_c$, much larger than the expected weak-coupling BCS value ($1.74 k_B T_c$), thus suggesting *strongly-coupled* [49] Cooper pairs in W_3Al_2C . This is confirmed also by the specific-heat discontinuity at T_c , i.e., $\Delta C/\gamma T_c$, here around 2.5–2.7, which is higher than 1.43 predicted by the BCS theory.

3.3. Comparison with other members of the M_3X_2Y family

The superconducting properties of the M_3X_2Y family of NCSCs are summarized in table 1. The data are somewhat challenging to interpret, because of the lack of a clear trend when arranged in order of increasing atomic number $Z(M)$. Most likely this reflects the fact that the superconducting behaviour of the M_3X_2Y compounds is highly dependent on the details of their band structure, which differs widely between members of the same family. Despite this difficulty, we can still draw some conclusions.

First, we note that the SC gap values $2\Delta/k_B T_c$ seem to differ, depending on whether they were determined by means of NMR, μ SR, or C_p measurements. In general, the gaps estimated via NMR and μ SR, which are both local-probe techniques, tend to be in good agreement. Conversely, the SC gaps determined from C_p data tend to be higher than those calculated from NMR and μ SR data, and systematically indicate a strong electron-phonon coupling across the entire family of M_3X_2Y compounds.

Secondly, we note that the $(T_1 T)^{-1}$ values of W_3Al_2C are consistent with those of the analog compound Mo_3Al_2C obtained by Bauer et al [18]. Since Mo_3Al_2C adopts the same structure as W_3Al_2C , the only differences being that W is less electronegative than Mo (1.7 vs 2.16 on the Pauling scale) and the marginally larger atomic covalent radius of the W atoms compared to Mo (150 vs 145 pm),

Parameter	Rh ₂ Mo ₃ N	Mo ₃ Al ₂ C	Li ₂ Pd ₃ B	W ₃ Al ₂ C	Li ₂ Pt ₃ B
$Z(M)$	42	42	46	74	78
T_c (K)	4.3 [43]	9.0 [18]	7.2 [44]	7.6 [11]	2.6 [44]
γ (mJ/mol K ²)	24.15 [43]	17.8 [18]	9.5 [44]	10	9.6 [44]
$\Delta C_p/\gamma T_c$	1.5	2.28 [18]	1.75 [44]	2.3	0.75 [44]
ξ (nm)	6.77 [43]	4.6 [18]	7.6 [44]	<5.7 [11]	11.8 [44]
$N(E_F)$ (states/eV/f.u.)	—	5.48 [18]	2.24 [45]	2.37 [11]	2.9 [45]
$1/(T_1 T)$ (sK) ⁻¹	—	0.34(²⁷ Al)[14] 0.075(²⁷ Al)[18] 0.012(²⁷ Al)[19]	0.045(¹¹ B)[21]	0.017(²⁷ Al)	0.034(¹¹ B)[21]
$2\Delta/k_B T_c$ (C_p)	3.62 [43]	4.03 [13]	—	4.50	non <i>s</i> -wave
$2\Delta/k_B T_c$ (NMR)	—	2.8 [14]	2.2 [8]	3.5	non <i>s</i> -wave
$2\Delta/k_B T_c$ (μ SR)	3.46 (dirty) [46] 3.84 (clean) [46]	2.59 [20]	—	3.5 [12]	non <i>s</i> -wave

Table 1. Comparison of the superconducting parameters of selected noncentrosymmetric superconductors with the chemical formula M_3X_2Y , where M is a metal. In all the cited references, $N(E_F)$ includes the contribution from SOC.

we expect the $N(E_F)$ of Mo₃Al₂C and W₃Al₂C to be of a similar magnitude and, consequently, their $(T_1 T)^{-1}$ values to be comparable. Considering that the $N(E_F)$ of Mo₃Al₂C is twice as large as that of W₃Al₂C (5.48 vs 2.37, see table 1), this results in an approximately fourfold increase in relaxation rate [$(T_1 T)^{-1} = 0.075$ vs 0.017 (sK)⁻¹, see table 1]. On the other hand, the $(T_1 T)^{-1}$ values obtained by Kuo et al [19] and Koyama et al [14] are wildly different (see figure 6). Recently, it was shown that the deliberate introduction of vacancies (here Al) in M_3X_2Y by soft chemical etching does not significantly influence the density of states (as from DFT calculations and heat-capacity data), but instead it dramatically alters the strength of electron-phonon coupling [41]. Hence, the presence of vacancies might justify the different $(T_1 T)^{-1}$ values obtained by the different groups. Furthermore, since W₃Al₂C intrinsically contains more Al-vacancies than its Mo counterpart [41], this might explain the BCS-type character of the former.

Thirdly, our results in table 1 support the observation made by Bauer et al [1] that, in case of phonon-mediated superconductors, although a noncentrosymmetric crystalline structure is required for the occurrence of unconventional superconductivity, it does not necessarily imply it. Another remarkable example of this is Mo₃P [50] which, as W₃Al₂C reported here, is a normal BCS-type superconductor, despite being an NCSC. Further, even within the same family, isostructural compounds can display a different superconducting behavior. For instance, CePt₃Si and LaPt₃Si are isostructural ($P4mm$ space group) and both display a large SOC. However, while CePt₃Si exhibits unconventional superconductivity [51, 52], LaPt₃Si does not [52]. Future studies could shed more light on this issue and clarify the link between unconventional SC and the lack of a structural inversion center.

4. Conclusion

Extensive NMR- and specific-heat measurements in the noncentrosymmetric W₃Al₂C superconductor, provide ample evidence about its weak electron correlation, yet with a strong electron-phonon coupling. Most importantly, we establish that W₃Al₂C shows a conventional BCS-type *s*-wave superconductivity. This, apparently unnoteworthy result, is surprising in view of the enhanced SOC of W atoms, whose 5*d* orbitals dominate the density of states at the Fermi level. This is all the more remarkable, if one considers that the analogous Mo₃Al₂C compound, hosting the much lighter Mo atoms, is claimed to be an unconventional superconductor. Such a counterintuitive outcome may be explained with the subtle role played by spin-orbit coupling, as well as by its competition with the electron bandwidth in the M_3X_2Y family. Finally, by considering the similar case of Mo₃P, we show that W₃Al₂C represents yet another example of a noncentrosymmetric material with conventional normal-state- and superconducting properties, thus emphasizing the role of a noncentrosymmetric structure as a beneficial (but not sufficient) condition in achieving unconventional superconductivity.

5. Acknowledgements

T.S. acknowledges support from the Natural Science Foundation of Shanghai (Grants No. 21ZR1420500 and 21JC1402300). This work was partially supported by the Schweizerische Nationalfonds zur Förderung der Wissenschaftlichen Forschung, SNF (Grant no. 200021-169455). Y.P. Qi was supported by the National Natural Science Foundation of China (Grants No. U1932217 and 11974246) and the Science and Technology Commission of Shanghai Municipality (19JC1413900).

6. References

- [1] Bauer E and Sigrist M (eds) 2012 *Non-Centrosymmetric Superconductors* vol 847 (Berlin: Springer Verlag)
- [2] Smidman M, Salamon M B, Yuan H Q and Agterberg D F 2017 *Rep. Prog. Phys.* **80** 036501
- [3] Anderson P W 1984 *Phys. Rev. B* **30**(7) 4000–4002
- [4] Joynt R and Taillefer L 2002 *Rev. Mod. Phys.* **74** 235 and references therein
- [5] Luke G M, Keren A, Le L P, Wu W D, Uemura Y J, Bonn D A, Taillefer L and Garrett J D 1993 *Phys. Rev. Lett.* **71** 1466
- [6] Schemm E R, Gannon W J, Wishne C M, Halperin W P and Kapitulnik A 2014 *Science* **345** 190
- [7] Norman M R 2011 *Science* **332** 196–200
- [8] Nishiyama M, Inada Y and Zheng G q 2005 *Phys. Rev. B* **71**(22) 220505
- [9] Shimamura A, Furukawa Y, Kumagai K, Takeya H and Hirata K 2007 *Physica C* **460–462** 663–665
- [10] Yuan H Q, Agterberg D F, Hayashi N, Badica P, Vandervelde D, Togano K, Sigrist M and Salamon M B 2006 *Phys. Rev. Lett.* **97**(1) 017006
- [11] Ying T P, Qi Y P and Hosono H 2019 *Phys. Rev. B* **100**(9) 094522
- [12] Gupta R, Ying T P, Qi Y P, Hosono H and Khasanov R 2021 *Phys. Rev. B* **103**(17) 174511
- [13] Karki A B, Xiong Y M, Vekhter I, Browne D, Adams P W, Young D P, Thomas K R, Chan J Y, Kim H and Prozorov R 2010 *Phys. Rev. B* **82**(6) 064512
- [14] Koyama T, Maeda Y, Yamazaki T, Ueda K, Mito T, Kohara T, Waki T, Tabata Y, Tsunemi H, Ito M and Nakamura H 2013 *J. Phys. Soc. Jpn.* **82** 073709
- [15] Koyama T, Ozaki Y, Ueda K, Mito T, Kohara T, Waki T, Tabata Y, Michioka C, Yoshimura K, Suzuki M T and Nakamura H 2011 *Phys. Rev. B* **84**(21) 212501
- [16] Bonalde I, Kim H, Prozorov R, Rojas C, Rogl P and Bauer E 2011 *Phys. Rev. B* **84**(13) 134506
- [17] Zhigadlo N D, Logvinovich D, Stepanov V A, Gonnelli R S and Daghero D 2018 *Phys. Rev. B* **97**(21) 214518
- [18] Bauer E, Rogl P, Chen X Q, Khan R T, Michor H, Hilscher G, Royanian E, Kumagai K, Li D Z, Li Y Y, Podloucky R and Rogl P 2010 *Phys. Rev. B* **82**(6) 064511
- [19] Kuo C N, Liu H F and Lue C S 2012 *Phys. Rev. B* **85**(5) 052501
- [20] Bauer E, Sekine C, Sai U, Rogl P, Biswas P K and Amato A 2014 *Phys. Rev. B* **90**(5) 054522
- [21] Nishiyama M, Inada Y and Zheng G q 2007 *Phys. Rev. Lett.* **98**(4) 047002
- [22] Rodríguez-Carvajal J 1993 *Physica B: Condens. Matter* **192** 55
- [23] McDowell A F 1995 *J. Magn. Reson. Ser. A* **113** 242–246
- [24] Alloul H 2015 *Scholarpedia* **10** 30632
- [25] Narayanan A, Hartman J S and Bain A D 1995 *J. Magn. Reson. Ser. A* **112** 58–65
- [26] Carter G C, Bennett L H and Kahan D J 1977 *Metallic shifts in NMR: A review of the theory and comprehensive critical data compilation of metallic materials (Progr. Mater. Sci. vol 20)* (Oxford: Pergamon Press)
- [27] Bennett L H, Watson R E and Carter G C 1970 *J. Res. Nat. Bur. Stand.* **74A** 569–610
- [28] Mehring M and Raber H 1973 *Solid State Commun.* **13** 1637–1639
- [29] Sandor M T, Kecskes L J, He Q, Xu J and Wu Y 2011 *Chin. Sci. Bull.* **56**(36) 3937–3941 and references therein
- [30] Korrinda J 1950 *Physica* **16**(7) 601–610
- [31] Hebel L C and Slichter C P 1957 *Phys. Rev.* **107**(3) 901–902
- [32] Hebel L C and Slichter C P 1959 *Phys. Rev.* **113**(6) 1504–1519
- [33] Hebel L C 1959 *Phys. Rev.* **116**(1) 79–81
- [34] Alloul H 2014 *Scholarpedia* **9** 32069
- [35] Goldberg I B, Ehrenfreund E and Weger M 1968 *Phys. Rev. Lett.* **20**(11) 539–540
- [36] Shiroka T, Casola F, Glazkov V, Zheludev A, Prša K, Ott H R and Mesot J 2011 *Phys. Rev. Lett.* **106**(13) 137202
- [37] Shiroka T, Eggenchwiler F, Ott H R and Mesot J 2019 *Phys. Rev. B* **99**(3) 035116
- [38] Li Z, Jiao W H, Cao G H and Zheng G q 2016 *Phys. Rev. B* **94**(17) 174511
- [39] Bardeen J, Cooper L N and Schrieffer J R 1957 *Phys. Rev.* **108**(5) 1175–1204
- [40] Ding Q P, Wiecki P, Anand V K, Sangeetha N S, Lee Y, Johnston D C and Furukawa Y 2016 *Phys. Rev. B* **93**(14) 140502
- [41] Ying T, Muraba Y, Iimura S, Yu T, Cheng P, Kamiya T, Lu Y, Li J, Qi Y and Hosono H 2020 *iScience* **23** 101196
- [42] Tinkham M 1996 *Introduction to Superconductivity* 2nd ed (Mineola, NY: Dover Publications)
- [43] Wei W, Zhao G J, Kim D R, Jin C, Zhang J L, Ling L, Zhang L, Du H, Chen T Y, Zang J, Tian M, Chien C L and Zhang Y 2016 *Phys. Rev. B* **94**(10) 104503
- [44] Takeya H, Kasahara S, El Massalami M, Mochiku T, Hirata K and Togano K 2007 *Mater. Sci. Forum* **561–565** 2079–2082
- [45] Lee K W and Pickett W E 2005 *Phys. Rev. B* **72**(17) 174505
- [46] Shang T, Smidman M, Ghosh S K, Baines C, Chang L J, Gawryluk D J, Barker J A T, Singh R P, Paul D M, Balakrishnan G, Pomjakushina E, Shi M, Medarde M, Hillier A D, Yuan H Q, Quintanilla J, Mesot J and Shiroka T 2018 *Phys. Rev. Lett.* **121** 257002
- [47] Padamsee H, Neighbor J E and Shiffman C A 1973 *J. Low Temp. Phys.* **12** 387
- [48] Carrington A and Manzano F 2003 *Physica C* **385** 205
- [49] Rainer D and Sauls J A 1995 *Strong-coupling theory of superconductivity* (Singapore: World Scientific) chap 2, pp 45–78
- [50] Shang T, Philippe J, Verezhak J A T, Guguchia Z, Zhao J Z, Chang L J, Lee M K, Gawryluk D J, Pomjakushina E, Shi M, Medarde M, Ott H R and Shiroka T 2019 *Phys. Rev. B* **99**(18) 184513
- [51] Bauer E, Hilscher G, Michor H, Paul C, Scheidt E W, Gribanov A, Seropegin Y, Noël H, Sigrist M and Rogl P 2004 *Phys. Rev. Lett.* **92**(2) 027003
- [52] Ribeiro R L, Bonalde I, Haga Y, Settai R and Ōnuki Y 2009 *J. Phys. Soc. Jpn.* **78** 115002